ChemPubSoc Europe

DOI: 10.1002/cssc.201901309

CHEMSUSCHEM Full Papers

VIP *Very Important Paper*

Nitride-Derived Copper Modified with Indium as a Selective and Highly Stable Catalyst for the Electroreduction of Carbon Dioxide

Florentine L. P. Veenstra, Antonio J. Martín, and Javier Pérez-Ramírez*[a]

The lack of efficient catalysts prevents the electrocatalytic reduction of carbon dioxide from contributing to the pressing target of a carbon-neutral economy. Indium-modified copper nitride was identified as a stable electrocatalyst selective toward CO. In_2O_3/Cu_3N showed a Faradaic efficiency of 80% at 0.5 V overpotential for at least 50 h, in stark contrast to the very limited stability of the benchmark In_2O_3/Cu_2O. Microfabricated systems allowed to correlate activity with highly stable interfaces in indium-modified copper nitride. In contrast, fast diffusion of indium resulted in rapidly evolving interfaces in the case of the system based on oxide-derived Cu. A metastable nitrogen species observed by spectroscopic means was proposed as the underlying cause leading to the unchanging interfaces. This work reveals the stabilizing properties of nitride-derived copper toward high-performance multicomponent catalysts.

Introduction

The Paris agreement[1] established a roadmap to reduce the atmospheric concentration of CO_2 below 350 ppm within this century, including the important milestone of achieving a carbon-neutral economy by 2050. The electrocatalytic CO_2 reduction reaction (eCO_2RR) has the potential to abate anthropogenic emissions significantly within this pressing deadline, given its natural coupling with renewable energy sources and mild operating conditions. However, this vision faces the key challenge of developing selective, active, and stable electrocatalysts in aqueous media.[2] The emergence of synergistic effects in multicomponent systems provides unique opportunities to overcome the scaling relation[3,4] between the binding energies of intermediates inherently limiting the performance of transition metals typically used for this reaction.[5,6] However, a limited understanding of interfacial effects frequently accompanied by deep compositional and/or structural changes under reaction conditions[7–11] precludes the derivation of accurate structure–performance relationships that can guide the optimization toward breakthrough advances.

We recently demonstrated that the controlled variation of the geometry and composition achieved by microfabrication tools can be used to derive correlations with catalytic performance, monitor dynamic processes, and gain insights into the nature of the active phase in multicomponent electrocatalysts.[12] In particular, for the highly selective Cu–In system[7,13] a direct relationship between the amount of a Cu–In bimetallic phase with low indium content and the CO partial current density was disclosed when Cu_2O acted as the copper source, irrespective of the initial indium phase (In or In_2O_3). Moreover, its formation could be associated with a solid-state reaction developed under eCO_2RR conditions manifested in diffusion of indium through the copper matrix. The reason for the crucial role of the oxidic copper phase remains unclear but may be associated with any of the diverse features linked to Cu_2O reduced under eCO_2RR conditions (also called oxide-derived Cu, OD-Cu), such as a rougher surface,[14] larger density of grain boundaries[15,16] and the possible presence of residual oxygen[17,18] under operation conditions, which may also lead to characteristic electronic properties favoring the eCO_2RR.[19] These results explain the marked reconstruction under reaction conditions observed in In_2O_3 supported on Cu_2O (In_2O_3/Cu_2O)[8] but also stress the difficulty in achieving, through rational optimization, a configuration with high performance over prolonged operation. Because this is one of the most prominent standing challenges toward practicality in the eCO_2RR,[5,20] these results pose the question of whether a highly active and stable phase can be achieved by modifying the copper source.

To investigate this, we explored copper nitride (Cu_3N), a copper phase with a slightly more covalent character than Cu_2O,[21] which has been reported to display synergetic interactions with Cu in a core–shell (Cu_3N–Cu) configuration, favoring the selectivity toward C_{2+} products in the eCO_2RR as the result of Cu^+–Cu^0 interactions.[22] Catalytic tests over In_2O_3/Cu_3N yielded improved activity and selectivity toward CO and an excellent structural and catalytic stability for at least 50 h. This

[a] *F. L. P. Veenstra, Dr. A. J. Martín, Prof. J. Pérez-Ramírez*
Institute for Chemical and Bioengineering
Department of Chemistry and Applied Biosciences
ETH Zürich
Vladimir-Prelog-Weg 1, 8093 Zürich (Switzerland)www.ace.ethz.ch
E-mail: jpr@chem.ethz.ch

Supporting Information and the ORCID identification number(s) for the author(s) of this article can be found under: https://doi.org/10.1002/cssc.201901309.

behavior was rationalized over microfabricated electrodes, the analysis of which unambiguously associated eCO_2RR activity and interface but did not observe diffusion of indium in the case of In_2O_3/Cu_3N, giving rise to stable interfaces. In stark contrast, typical diffusion lengths of a few micrometers were found over the system based on OD-Cu. Spectroscopic analyses disclosed temporary persistent nitrogen species upon reduction, which may be associated to the stable behavior. This work thus unveils indium-modified copper nitride as a novel, selective, and robust catalyst and underlines the potential of reduced copper nitride (nitride-derived Cu, ND-Cu) to develop synergistic effects in the eCO_2RR.

Results and Discussion

High stability and selectivity of indium-modified copper nitride

We aimed to enhance the modest structural stability of the In_2O_3/Cu_2O system[7] by replacing copper oxide by copper nitride without negatively affecting its high selectivity. We took as reference the catalyst In_2O_3/Cu_2O in powder form with 7.2 wt% indium reported by us previously with approximately 65% Faradaic efficiency (FE) toward CO at −0.6 V vs. reversible hydrogen electrode (RHE).[23] We prepared series of In_2O_3/Cu_2O and In_2O_3/Cu_3N materials with nominal loadings of 0.5, 1.5, and 4 wt% In by calcination of $In(OH)_3$ supported on Cu_2O or Cu_3N (see the Experimental Section). XRD patterns (Figure 1a) confirmed the successful formation of the nitride phase, although no reflection associated to indium phases could be identified owing to the low loading (Table S1 in the Supporting Information) and high dispersion observable in the scanning transmission electron microscopy (STEM) coupled to energy-dispersive X-ray spectroscopy (EDXS) elemental maps (Figure 1b). Reflections associated to In_2O_3 were nonetheless visible in oxide-based counterparts (Figure S1 in the Supporting Information), likely owing to the slightly larger average particle size (Figure 1b). In all cases the catalysts presented a similar surface structure composed of sub-micrometric features (Figure S2 in the Supporting Information).

The powders were deposited on the microporous layer of a technical carbon gas-diffusion layer (GDL) electrode prior to electrolysis by airbrushing. We first evaluated the catalytic properties of the copper oxide and copper nitride supports, which yielded very modest eCO_2RR activity (Figure 2a). A remarkably high FE toward CO of approximately 80% as the only carbon product was achieved over In_2O_3/Cu_3N with 1.7 wt% indium. This surpassed the best-performing oxide-based system, which also promoted formation of formate, likely reflecting the catalytic nature of the oxide support and/or surface enrichment of indium,[24] as strongly suggested by the characteristic redox peaks of the In/In_2O_3 pair[24] (≈−0.45 V and −0.05 V in Figure 2b). In turn, this result suggests metallic indium as the predominant indium phase under the operation potential (−0.6 V). Strikingly, both materials largely diverged in terms of catalytic stability (Figure 2c and Figure S3 in the Supporting Information). An extended catalytic test over 50 h showed stable activity and selectivity over In_2O_3/Cu_3N, retaining approximately 90% of the initial FE by the end of the experiment. In contrast, the benchmark In_2O_3/Cu_2O exhibited lower currents and an early deactivation pattern. We remark that long-term stability studies for CO production have been primarily focused on silver-based systems so far, in view of the marked instability and/or poor scalability of the rest of high-performing materials.[20] After these observations, we concluded that the copper nitride phase is able to provide the Cu–In

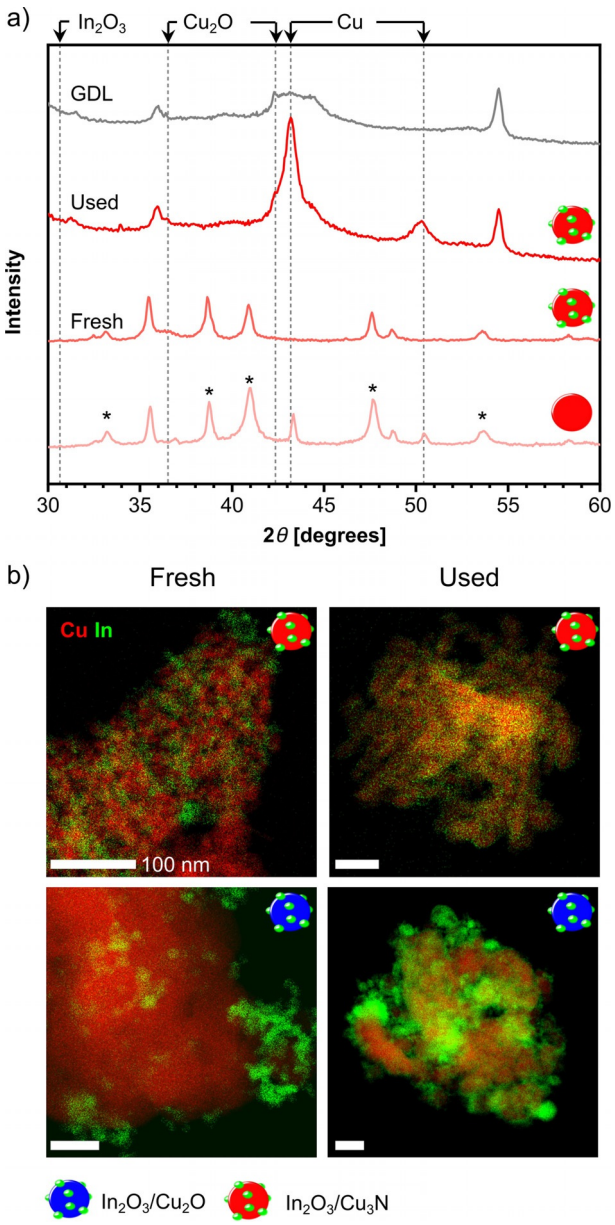

Figure 1. a) XRD patterns of fresh and used In_2O_3/Cu_3N (1.7 wt% In). The patterns of Cu_3N over which indium oxide was deposited and that of the underlying carbon-based GDL for the case of the used catalyst are provided for reference. The asterisks indicate reflections associated with Cu_3N. The positions of the main reflections for other relevant phases are indicated. b) Elemental mapping obtained by STEM-EDXS showing the distribution of indium over the copper phases prior to and post-reaction. Separated maps for Cu and In in the case of In_2O_3/Cu_3N are presented in Figure S4 in the Supporting Information to facilitate the visualization of the In distribution.

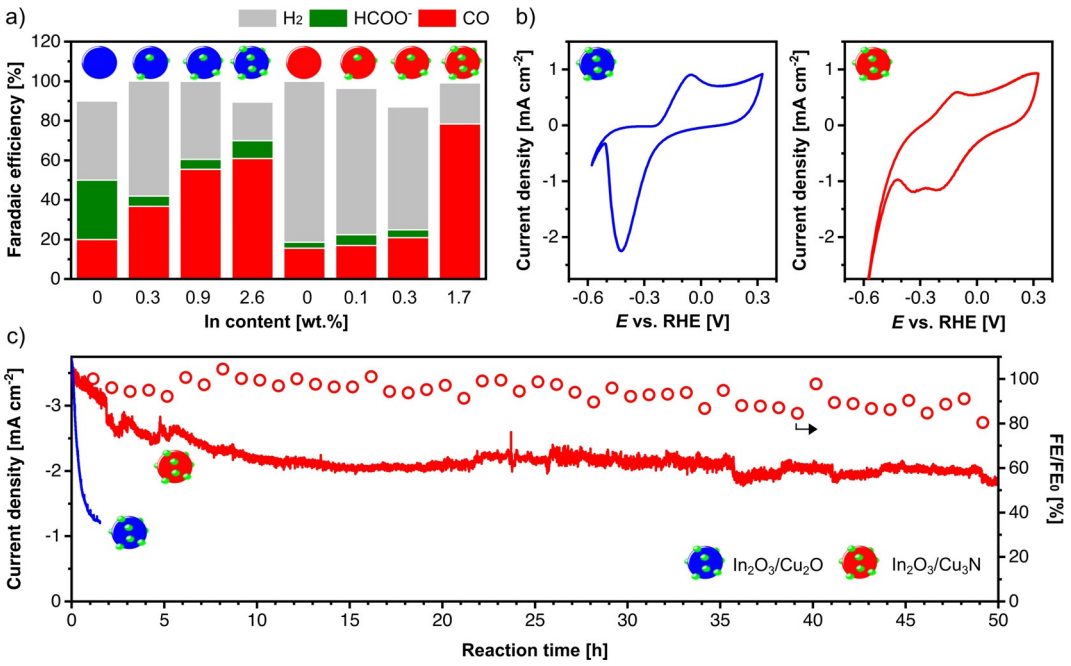

Figure 2. Catalytic evaluation and electrochemical characterization of materials in powder form. a) Product distribution over Cu_2O and Cu_3N unmodified and modified with indium oxide for different indium loadings; b) redox response after catalytic tests showing the characteristic In/In_2O_3 redox peaks more prominently in the case of In_2O_3/Cu_2O; c) evolution of the current density and percentage of the initial FE toward CO retained for In_2O_3/Cu_2O (2.6 wt% In) and In_2O_3/Cu_3N (1.7 wt% In) in an extended test. Operation conditions: chronoamperometry at −0.6 V vs. RHE in 0.1 M $KHCO_3$ saturated with CO_2 (pH 6.7).

system with a remarkable conjunction of high stability and selectivity.

XRD patterns after reaction did not reveal fundamental differences between the oxide- and nitride-based systems, displaying the bulk reduction of Cu_3N to metallic Cu (ND-Cu) under reaction conditions, in analogy to the OD-Cu arising from Cu_2O (Figure 1a and Figure S1 in the Supporting Information). The presence of reflections assigned to In_2O_3 in the used In_2O_3/Cu_2O (Figure S1 in the Supporting Information) must be associated with the rapid oxidation that metallic indium undergoes when exposed to the atmosphere. The formation of intermetallic compounds after reaction could not be directly assessed by XRD owing to the small concentration of In, although small unassigned reflections between 35 and 40° 2θ in In_2O_3/Cu_2O might be tentatively assigned to either CuIn (JCPDS 35-1150) or Cu_2In (JCPDS 42–1475). In regard to the distribution of indium over the used In_2O_3/Cu_3N, Figure 1b and Figure S4 in the Supporting Information show how the high initial dispersion of indium was retained after reaction, whereas over In_2O_3/Cu_2O the redistribution of indium during operation caused homogeneous coating over extensive areas of the OD-Cu support, in line with the redox response (Figure 2b). The positive influence of the nitride copper source in the stability of the system called for further investigations, which we initiated by assessing the unmodified oxide and nitride phases under reaction conditions.

Evolution of the unmodified copper nitride

The reduction of Cu_2O under eCO_2RR conditions to OD-Cu has been widely reported as a prerequisite for its outstanding catalytic properties.[16,26,27] OD-Cu displays a rougher surface favoring high local pH values[14] and abundance of grain boundaries[28] and atomic defects[27,29] which may be related to the favored diffusion of indium we observed in our previous work.[12] In view of this and the foreseeable similarities between the nitride and oxide phases, prior to analyzing interfacial effects we turned to analyze the evolution of copper nitride under operation conditions and compare it on the light of the oxide.

We studied sputtered films allowing fine control over the thickness and composition of metallic copper, copper oxide, and copper nitride. The surface of the as-deposited films of metallic and oxidic copper exhibited a similar aspect under SEM analysis comprising 30–50 nm particles (Figure 3a), the expected composition of which was confirmed by their XRD patterns (Figure S5 in the Supporting Information). In contrast, partially overlapping pyramidal particles formed the surface of the nitride film, clarifying its larger electrochemical double-layer capacitance (Figure S6 in the Supporting Information). Upon exposure to eCO_2RR conditions, XRD patterns indicated the exclusive presence of metallic Cu in all cases (Figure S5 in the Supporting Information), whereas micrographs displayed almost no effect of the eCO_2RR on the morphology of the metallic Cu, in contrast with the more open structure observed on the OD-Cu and ND-Cu (Figure 3a). Further insights followed from inspection of the current density evolution (Figure 3b). Metallic copper yielded a monotonically decreasing current throughout the experiment, whereas Cu_2O and Cu_3N showed a clear reduction peak at 10–20 s followed by gradual equilibration. Interestingly, the evolution of interparticle space obtained from analysis of SEM images at different times could link these observations (Figure 3c). The structure of the nitride and oxide

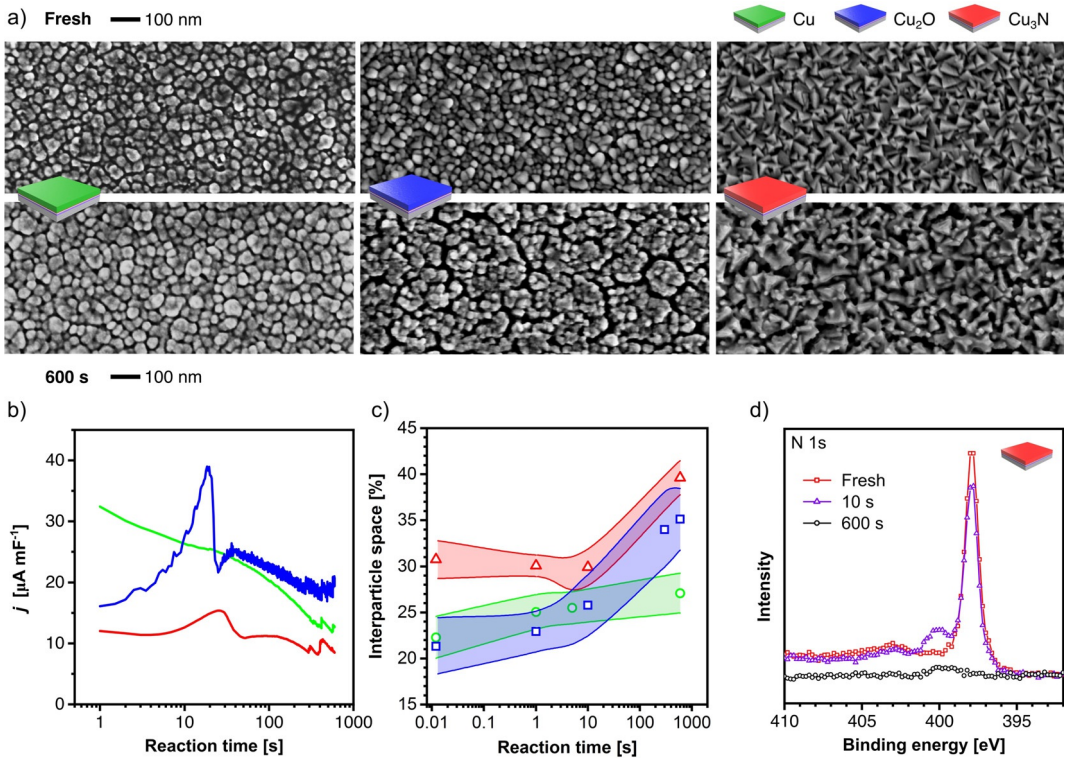

Figure 3. Evolution of unmodified copper phase films under eCO_2RR conditions. a) Micrographs of the as-deposited substrates and after exposure to reaction conditions for 600 s; b) evolution of the current normalized by double-layer capacitance (see Figure S6 in the Supporting Information); c) evolution of the interparticle space quantified as the percentage of black areas in the micrographs (the bands indicate the standard deviation of 10 spots); d) evolution of the N 1s signal obtained by XPS analysis of the copper nitride film at different reaction times.

layers opens upon the reduction peak and continues until the process stabilizes after approximately 300 s, thus providing the temporal frame during which the reconstruction takes place. After 10 s, the fraction of interparticle space on ND-Cu and OC-Cu partially converged.

In this respect, photoelectron emission around the N 1s provided further support to understand the reduction process of Cu_3N (Figure 3 d). The sharp peak at approximately 397.7 eV in the fresh material corresponds to the BE of nitrogen in Cu_3N[30] and decreases gradually over the course of the experiment until it becomes undetectable after 600 s, supporting the complete reduction to metallic Cu on the surface. Nonetheless, the fingerprint of a different nitrogen species at approximately 400 eV emerges after 10 s and seems to endure to a very limited extent until the end of the experiment. A similar state has been observed during the thermal decomposition of Cu_3N into Cu and N_2 and tentatively assigned to Cu_4N, the formation of which would be facilitated by the relatively easy diffusion of nitrogen in the copper lattice.[30,31] We mention the difficulty to assess ex situ the complete reduction of Cu_2O owing to the rapid reoxidation of OD-Cu upon exposure to the atmosphere.[32]

In summary, we found parallels between the evolution of copper oxide and nitride under eCO_2RR conditions toward OD-Cu and ND-Cu, respectively, although the presence of a small amount of persistent nitrogen with a different chemical nature formed during the reduction was revealed. This picture made it reasonable to expect comparable synergistic mechanisms between the nitride or the oxide substrates and the indium oxide.

Interfacial activity and stability in indium-modified copper nitride

As the next step, we aimed to understand the nature and the formation mechanism of the active phase in this new material. In view of the complexity of the Cu–In system, which makes it poorly accessible to detailed theoretical and/or in situ studies,[33] we approached this task by applying microfabrication tools.[12] Microfabricated catalysts display a drastic reduction of the uncertainty in terms of composition and structure compared to powder forms. Moreover, the high throughput at which they can be prepared and their easier integration with characterization techniques make them a promising model platform for the understanding of multicomponent catalysts.

Herein we apply this approach (Figure 4) to impose microstructure to the systems under study targeting electrodes with well-defined interfacial density (see the Experimental Section). Microfabrication allowed the production of several sets of electrodes in a reduced timeframe with highly controlled composition and geometry consisting of periodic regular hexagonal arrays of circular islands (≈100 nm height, comprising the indium oxide) deposited on a homogeneous thin film (≈200 nm height, the copper-based component). The main geometrical design variable was the interfacial density ρ_{int} as the total length of the perimeter of the islands per unit area of

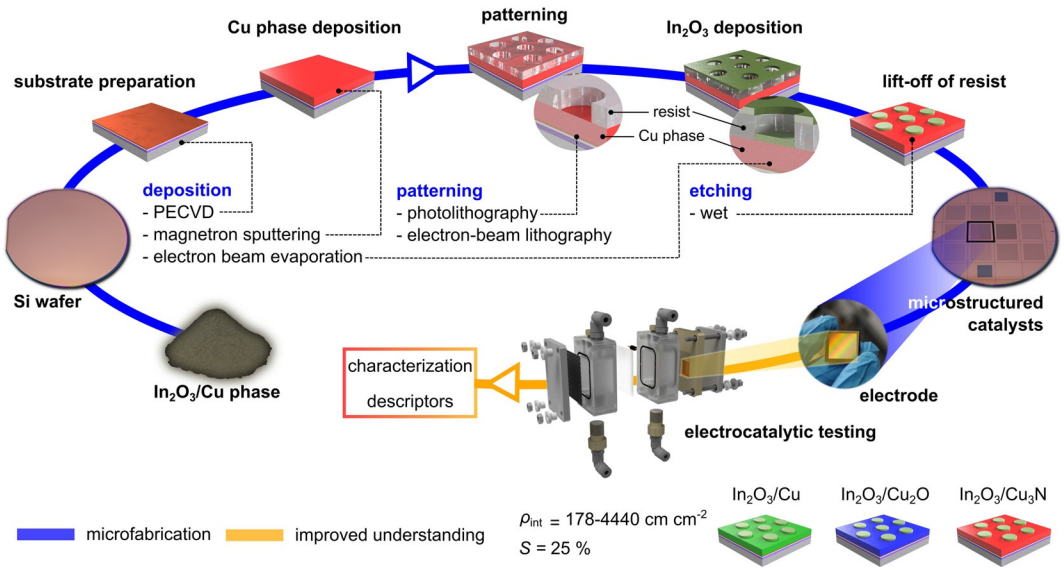

Figure 4. Microfabrication as an advanced tool to study interfacial effects in Cu–In systems. Indium oxide was patterned by microfabrication tools as a regular array of circular islands on different copper-based substrates with the aim of controlling ρ_{int} and keeping constant the coverage of the copper phase *S* (blue line). Prepared electrodes were tested under reaction conditions in a standard electrochemical setup. The controlled geometry allowed identification of performance descriptors and facilitated insight into the formation of the active phase (yellow line).

the electrode, which can be controlled by patterning a layer of photoresist through UV photolithography. With this geometry, the surface of the electrodes exposes three different possible active sites: the copper phase substrate, the indium oxide islands, and the interfacial ones, located at the perimeters. To differentiate interfacial contributions within the total measured activity, we designed electrodes spanning ρ_{int} over several orders of magnitude (178–4440 cm cm^{-2}) while keeping the same indium coverage of the copper substrate (≈25%, see the Supporting Information and Figure S7 therein). Low interfacial densities correspond to large islands and vice versa. In this manner, sets of electrodes (A_{total} = 2.25 cm^2) with three different compositions (denoted as island/surface) were prepared: (1) In_2O_3/Cu, (2) In_2O_3/Cu_2O, and (3) In_2O_3/Cu_3N. A more detailed information on the microfabrication process is available elsewhere[12] and in the Supporting Information.

The large geometrical active area of the structured electrodes allowed their direct electrochemical testing and the quantification of the gas-phase products with a standard electrochemical cell for eCO_2RR studies. The catalytic activity of In_2O_3/Cu electrodes (Figure 5) displayed low values comparable to the pure phases (see Figure S8 in the Supporting Information) irrespective of the interfacial density. Nonetheless, a different picture emerged from the In_2O_3/Cu_2O electrodes. The synergistic interaction at the interface between In_2O_3 and Cu_2O was clearly manifested by the larger activity and its positive correlation with the interfacial density,[12] which ceased at larger ρ_{int}, resulting in very low activity over electrodes with small islands (Figure 5). In stark contrast, the partial current density toward CO showed a consistent positive correlation with the interfacial density over In_2O_3/Cu_3N. These results confirmed the role of interfacial sites in the eCO_2RR activity in In_2O_3/Cu_3N and revealed the sensitivity of In_2O_3/Cu_2O to the spatial distribution of the phases. On a methodological note, we highlight the importance of homogenous current density, achieved by adding a thin Cu layer (10 nm) under the semiconducting Cu_3N and Cu_2O films (see Figure S9 in the Supporting Information and the Experimental Section).

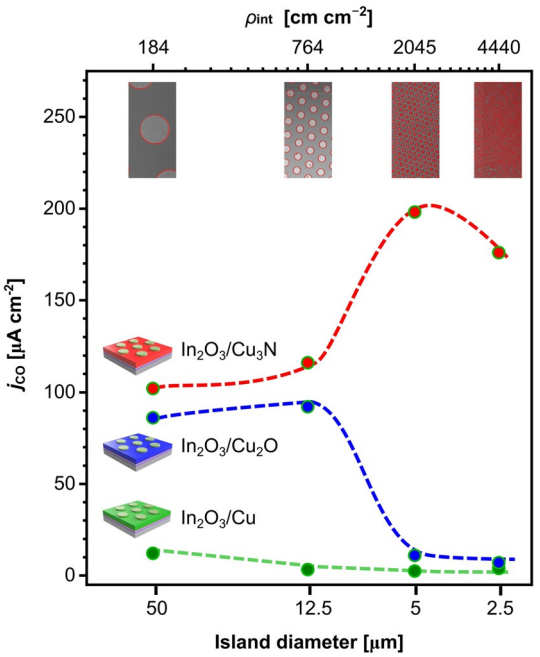

Figure 5. Electrocatalytic activity toward CO of microstructured multicomponent electrodes with different ρ_{int} controlled by preparing regular arrays of islands with different diameter and pitch. SEM images in which interfacial sites are highlighted in red are added for clarity. Operating conditions: −0.6 V vs. RHE in 0.1 M $KHCO_3$ saturated with CO_2 (pH 6.7) for 600 s.

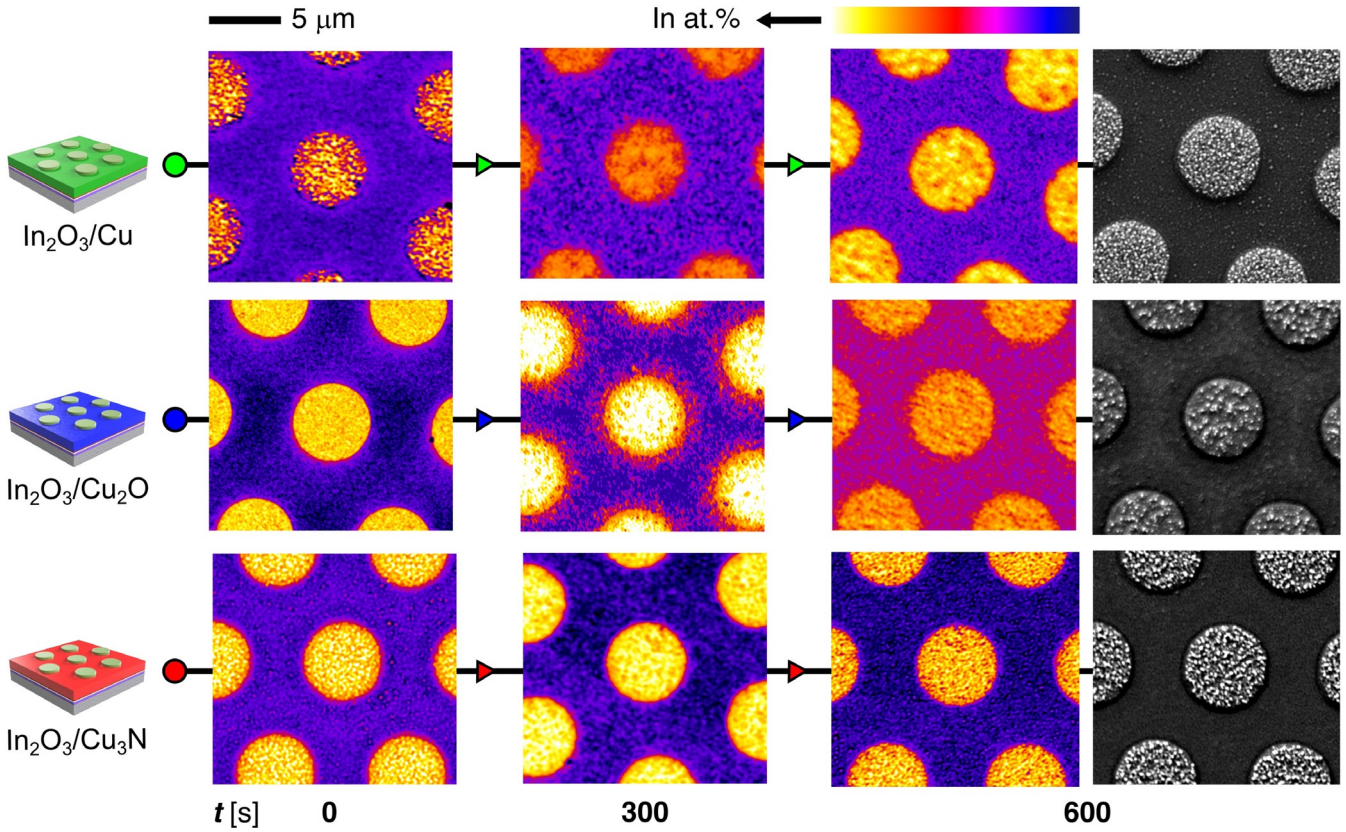

Figure 6. Evolution of the elemental distribution of indium obtained by SEM-EDXS at different reaction times in microfabricated electrodes. The corresponding SEM images after 600 s are added to confirm the structural stability of the islands in all cases.

In our previous study, we observed an appreciable diffusion of indium over In_2O_3/Cu_2O after 5 min under reaction conditions, giving rise to the Cu–In active phase.[12] In this study, we varied reaction times aiming to monitor its formation and facilitate the comparison with In_2O_3/Cu_3N. With this idea in mind, we carefully mapped the indium distribution by SEM-EDXS over the three fresh compositions and after reaction times of 300 and 600 s (Figure 6) for electrodes populated with 5 μm islands, on which catalytic performances differed more noticeably (Figure 5). The In_2O_3/Cu system showed no visible evolution of the interface, retaining the deposited indium within the perimeter of the islands at all reaction times. In the case of In_2O_3/Cu_2O, the diffusion of indium was clearly observable after 300 s, forming indium-containing halos around the individual islands associated with eCO_2RR activity.[12] However, after 600 s the halos merged, as reflected by the rather homogeneous and relatively rich distribution of indium among the islands. These observations at different times explained the direct relation between activity and interfacial density over electrodes with a larger pitch among islands. As the diffusion length of indium becomes closer to the pitch over electrodes with smaller islands at earlier times, the more active Cu–In phase (reasonably associated to the perimeter of the halos) might disappear upon merging of the halos, and the activity starts to resemble that of pure indium oxide (Figure S8 in the Supporting Information).

Notably, there was no evidence of this complex evolution process in the case of In_2O_3/Cu_3N. The diffusion of indium was not observable in this case, suggesting its restriction to the nanometre scale in case it exists. This result is in line with the retained dispersion after reaction observed over the powder form in Figure 1 b and the consistent activity–interfacial density trend found in Figure 5 because overlapping of indium-rich areas does not occur. In addition, SEM images ruled out deterioration of the electrode surface as the reason behind differences in performance (Figure 6).

At this point, evidence collected over the nature of the active sites in microfabricated electrodes and the catalytic results obtained over the powder counterparts (Figure 2) could be directly correlated. As the next step, we aimed to gain further insights into the reason behind the interfacial stability on the In_2O_3/Cu_3N material.

Metastable nitrogen species during the reduction of indium-modified copper nitride

We notice that even though the debate elucidating if OD-Cu contains remaining oxygen under operation conditions is still open, there is a consensus that it would be limited to trace levels and that the reduction process occurs rapidly.[14,17] In this context, the suggested presence of nitrogen species with a different chemical environment even after exposure to reaction conditions for 600 s in Cu_3N (Figure 3 d) advised some differen-

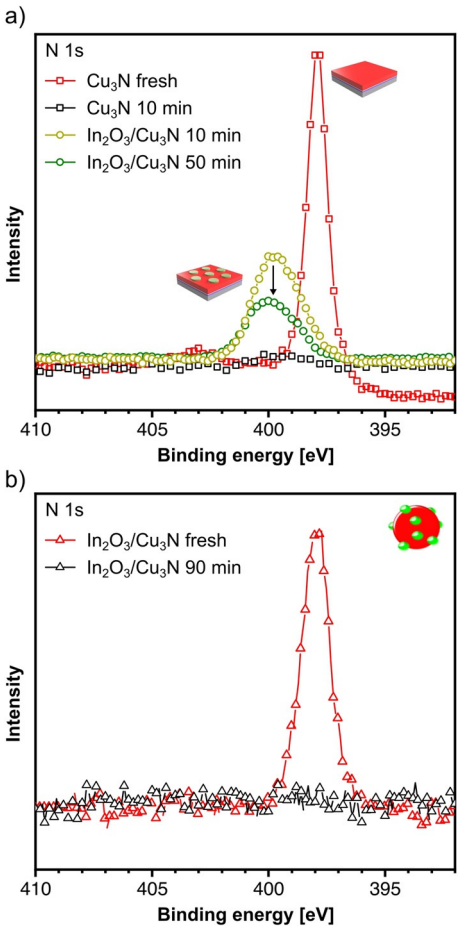

Figure 7. High-resolution XPS survey around the N 1s signal for In_2O_3/Cu_3N before and after reaction at different times a) for the microfabricated form (5 μm islands). The corresponding signals for the pure nitride phase are added as reference. b) For the powder form (1.7 wt% In). The peak at approximately 398 eV corresponds to the bulk Cu_3N phase.

ces between the two copper phases. To investigate this, we tracked the N 1s signal over the microfabricated In_2O_3/Cu_3N after different reaction times (Figure 7a). Similar to the case of Cu_3N, the peak at 397.7 eV disappeared after 600 s, confirming the complete transformation of the surface. However, the binding energy at approximately 400 eV we associated to a metastable state was clearly detectable. Notably, post-reaction analysis after a more prolonged test for 3000 s (50 min) showed a gradual decrease of this signal, suggesting that the depletion of nitrogen in the indium-modified copper nitride is markedly delayed compared with the pure phase.

The existence of an appreciable amount of nitrogen in the copper matrix during the reduction and reconstruction process can then be hypothesized to hamper the fast diffusion of indium observed during the reduction and reconstruction process over OD-Cu,[12] restricting the copper–indium interaction to the close vicinity of the islands. After stabilization of the surface and complete elimination of metastable nitrogen at sufficiently long reaction times, the diffusion of indium on metallic copper is expected to proceed at a very low rate at RT, according to our results over In_2O_3/Cu (Figure 6) and available reports.[34,35] However, the participation of electronic effects associated to Cu–In–N interactions cannot be discarded at this point. Similar analyses (Figure 7b) over the powder form in In_2O_3/Cu_3N with 1.7 wt% In evidenced the complete depletion of nitrogen in the electrode after exposure to eCO_2RR conditions for 90 min. In conjunction with the stable performance for 50 h exhibited in Figure 2c, this observation reveals that the presence of metastable nitrogen is not required for a stable extended operation, in line with the initial stabilizing effect of nitrogen proposed for the microfabricated system. However, we notice that the high stability displayed by the powder form can be also modulated by unaccounted phenomena not easily detectable over the microfabricated counterparts, which calls for further investigations on this matter.

In summary, the set of presented results indicates that In_2O_3/Cu_3N develops highly stable, active, and selective interfaces allowing for a stable operation, in contrast to the rapidly evolving oxide counterpart driven by the fast diffusion of indium (Figure 8). Even though the nitride phase is rapidly reduced and undergoes fast surface reconstruction, a considerable amount of nitrogen remains temporarily trapped in the lattice of the ND-Cu, likely stabilizing the copper–indium interface.

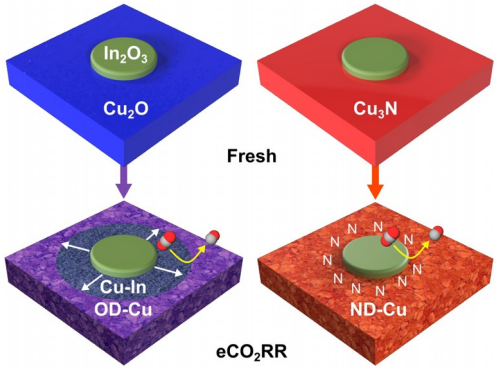

Figure 8. Configuration of the active phases under reaction conditions for In_2O_3/Cu_2O and In_2O_3/Cu_3N.

Conclusions

In_2O_3/Cu_3N emerged as a selective and highly stable electrocatalyst in the reduction of CO_2 to CO (eCO_2RR), outperforming the less stable oxide-based benchmark. The use of copper nitride eliminated the uncontrolled structural and compositional changes associated with the latter. The regular composition and structure of microstructured electrodes facilitated establishing a direct relation between the Cu–In interface in In_2O_3/Cu_3N and eCO_2RR activity, which was not accompanied by detectable indium diffusion into the copper matrix, as was the case of the oxide-based material. Spectroscopic evidence revealed the presence of metastable nitrogen under reaction conditions, which we associated with the improved interfacial stability. The findings reveal the potential of nitride-derived copper to engineer multicomponent systems with high efficiency for the eCO_2RR. In parallel, they underline microfabrication as a tool to establish synthesis–property–function relations in multicomponent systems for the range of electrocatalytic applications.

Experimental Section

Cu_3N was prepared through solid-state reaction between CuO and $NaNH_2$ under inert atmosphere at moderate temperature (Ar, 443 K, 60 h). Cu_2O was solvothermally synthesized from $Cu(NO_3)_2{\cdot}3H_2O$ (413 K, 10 h, in ethylene glycol). In_2O_3/Cu_3N and In_2O_3/Cu_2O with nominal indium loadings of 0.5, 1.5, and 4 wt% were prepared by calcination of $In(OH)_3/Cu_3N$ or $In(OH)_3/Cu_2O$, obtained by addition of excess NH_4OH to dissolved $InCl_3$ in the presence of Cu_3N or Cu_2O, respectively. Electrodes were prepared by airbrushing catalytic inks on GDL carbon papers (catalyst loading 0.5–1 mg cm^{-2}). Microfabricated electrodes were prepared on Si wafers. Preparation of the substrate included physical deposition of consecutive thin films of SiO_x (500 nm), Ta (50 nm), and Cu (10 nm). Subsequently, metallic Cu, Cu_2O, or Cu_3N (190 nm) was sputtered at RT. UV lithography was used to pattern negative resists with regular hexagonal arrays of circles with coincidental diameter and pitch (2.5, 5, 12.5, and 50 μm) to tune the interfacial density while keeping constant the coverage of the copper surface. After the development of the resist, In_2O_3 was deposited by evaporation (100 nm). The final electrodes (2.25 cm^2) were obtained after the lift-off of the remaining resist. Electrocatalytic tests were performed in 0.1 M $KHCO_3$ saturated with CO_2 at −0.6 V vs. RHE. Gaseous products were analyzed by on-line GC. Liquid products were analyzed by ^{1}H NMR spectroscopy. The structural and compositional properties of the catalysts were studied by XRD, XPS, and STEM coupled to EDXS. The other experimental details are presented in the Supporting Information.

Acknowledgements

This work was sponsored by the European Union through the A-LEAF project (732840-A-LEAF). The authors gratefully acknowledge the FIRST Center for Micro- and Nanoscience and the Scientific Center for Optical and Electron Microscopy (ScopeM) of ETH Zurich for access to their facilities. The authors are grateful to J. Meyet for continuous support on the synthesis of copper nitride, Dr. R. Hauert and S. Büchele for XPS measurements, E. Vorobyeva for microscopy measurements, Dr. R. Verel for NMR assistance, M. Singleton and Dr. F. Krogh for deposition assistance.

Conflict of interest

The authors declare no conflict of interest.

Keywords: carbon dioxide · copper nitride · electrochemistry · interfaces · microfabrication

[1] W. Steffen, K. Richardson, J. Rockström, S. E. Cornell, I. Fetzer, E. M. Bennett, R. Biggs, S. R. Carpenter, W. de Vries, C. A. de Wit, C. Folke, D. Gerten, J. Heinke, G. M. Mace, L. M. Persson, V. Ramanathan, B. Reyers, S. Sörlin, *Science* **2015**, *347*, 1259855.
[2] A. J. Martín, G. O. Larrazábal, J. Pérez-Ramírez, *Green Chem.* **2015**, *17*, 5114 – 5130.
[3] H. A. Hansen, J. B. Varley, A. A. Peterson, J. K. Nørskov, *J. Phys. Chem. Lett.* **2013**, *4*, 388 – 392.
[4] A. A. Peterson, F. Abild-Pedersen, F. Studt, J. Rossmeisl, J. K. Nørskov, *Energy Environ. Sci.* **2010**, *3*, 1311 – 1315.
[5] G. O. Larrazábal, A. J. Martín, J. Pérez-Ramírez, *J. Phys. Chem. Lett.* **2017**, *8*, 3933 – 3944.
[6] K. P. Kuhl, E. R. Cave, D. N. Abram, T. F. Jaramillo, *Energy Environ. Sci.* **2012**, *5*, 7050.
[7] S. Rasul, D. H. Anjum, A. Jedidi, Y. Minenkov, L. Cavallo, K. Takanabe, *Angew. Chem. Int. Ed.* **2015**, *54*, 2146 – 2150; *Angew. Chem.* **2015**, *127*, 2174 – 2178.
[8] G. O. Larrazábal, A. J. Martín, S. Mitchell, R. Hauert, J. Pérez-Ramírez, *ACS Catal.* **2016**, *6*, 6265 – 6274.
[9] Y. Huang, Y. Deng, A. D. Handoko, G. K. L. Goh, B. S. Yeo, *ChemSusChem* **2018**, *11*, 320 – 326.
[10] T. Shinagawa, G. O. Larrazábal, A. J. Martín, F. Krumeich, J. Pérez-Ramírez, *ACS Catal.* **2018**, *8*, 837 – 844.
[11] J. He, K. E. Dettelbach, D. A. Salvatore, T. Li, C. P. Berlinguette, *Angew. Chem. Int. Ed.* **2017**, *56*, 6068 – 6072; *Angew. Chem.* **2017**, *129*, 6164 – 6168.
[12] G. O. Larrazábal, T. Shinagawa, A. J. Martín, J. Pérez-Ramírez, *Nat. Commun.* **2018**, *9*, 1477.
[13] Z. B. Hoffman, T. S. Gray, K. B. Moraveck, T. B. Gunnoe, G. Zangari, *ACS Catal.* **2017**, *7*, 5381 – 5390.
[14] D. Gao, R. M. Arán-Ais, H. S. Jeon, B. R. Cuenya, *Nat. Catal.* **2019**, *2*, 198 – 210.
[15] C. W. Li, M. W. Kanan, *J. Am. Chem. Soc.* **2012**, *134*, 7231 – 7234.
[16] A. Verdaguer-Casadevall, C. W. Li, T. P. Johansson, S. B. Scott, J. T. McKeown, M. Kumar, I. E. L. Stephens, M. W. Kanan, I. Chorkendorff, *J. Am. Chem. Soc.* **2015**, *137*, 9808 – 9811.
[17] H. Mistry, A. S. Varela, C. S. Bonifacio, I. Zegkinoglou, I. Sinev, Y. W. Choi, K. Kisslinger, E. A. Stach, J. C. Yang, P. Strasser, B. R. Cuenya, *Nat. Commun.* **2016**, *7*, 12123.
[18] A. Eilert, F. Cavalca, F. S. Roberts, J. Osterwalder, C. Liu, M. Favaro, E. J. Crumlin, H. Ogasawara, D. Friebel, L. G. M. Pettersson, A. Nilsson, *J. Phys. Chem. Lett.* **2017**, *8*, 285 – 290.
[19] M. Favaro, H. Xiao, T. Cheng, W. A. Goddard III, J. Yano, E. J. Crumlin, *Proc. Natl. Acad. Sci. USA* **2017**, *114*, 6706 – 6711.
[20] O. G. Sánchez, Y. Y. Birdja, M. Bulut, J. Vaes, T. Breugelmans, D. Pant, *Curr. Opin. Green Sustainable Chem.* **2019**, *16*, 47 – 56.
[21] A. Zakutayev, *J. Mater. Chem. A* **2016**, *4*, 6742 – 6754.
[22] Z. Q. Liang, T. T. Zhuang, A. Seifitokaldani, J. Li, C. W. Huang, C. S. Tan, Y. Li, P. De Luna, C. T. Dinh, Y. Hu, Q. Xiao, P.-L. Hsieh, Y. Wang, F. Li, R. Quintero-Bermudez, et al., *Nat. Commun.* **2018**, *9*, 3828.
[23] G. O. Larrazábal, A. J. Martín, F. Krumeich, R. Hauert, J. Pérez-Ramírez, *ChemSusChem* **2017**, *10*, 1255 – 1265.
[24] J. L. White, A. B. Bocarsly, *J. Electrochem. Soc.* **2016**, *163*, H410 – H416.
[25] A. Dutta, M. Rahaman, N. C. Luedi, M. Mohos, P. Broekmann, *ACS Catal.* **2016**, *6*, 3804 – 3814.
[26] Y. Lum, J. W. Ager, *Nat. Catal.* **2019**, *2*, 86 – 93.
[27] R. G. Mariano, K. McKelvey, H. S. White, M. W. Kanan, *Science* **2017**, *358*, 1187 – 1192.
[28] D. Gao, I. Zegkinoglou, N. J. Divins, F. Scholten, I. Sinev, P. Grosse, B. R. Cuenya, *ACS Nano* **2017**, *11*, 4825 – 4831.
[29] R. Gonzalez-Arrabal, N. Gordillo, M. S. Martin-Gonzalez, R. Ruiz-Bustos, F. Agulló-López, *J. Appl. Phys.* **2010**, *107*, 103513.
[30] S. J. Patil, D. S. Bodas, A. B. Mandale, S. A. Gangal, *Thin Solid Films* **2003**, *444*, 52 – 57.
[31] D. Depla, J. Haemers, R. De Gryse, *Plasma Sources Sci. Technol.* **2002**, *11*, 91 – 96.
[32] Y. Lum, J. W. Ager, *Angew. Chem. Int. Ed.* **2018**, *57*, 551 – 554; *Angew. Chem.* **2018**, *130*, 560 – 563.
[33] A. D. Handoko, F. Wei, Jenndy, B. S. Yeo, Z. W. Seh, *Nat. Catal.* **2018**, *1*, 922 – 934.
[34] C. L. Yu, S. S. Wang, T. H. Chuang, *J. Electron. Mater.* **2002**, *31*, 488 – 493.
[35] D.-G. Kim, C.-Y. Lee, S.-B. Jung, *J. Mater. Sci. Mater. Electron.* **2004**, *15*, 95 – 98.

Manuscript received: May 14, 2019
Accepted manuscript online: June 3, 2019
Version of record online: June 24, 2019

